Proton Strength Functions from (p,n) Cross Sections*

C. H. JOHNSON, A. GALONSKY, AND J. P. ULRICH†
Oak Ridge National Laboratory, Oak Ridge, Tennessee
(Received October 17, 1957)

To an accuracy of ±10%, (p,n) total cross sections averaged over resonances have been measured from threshold to about 500 kev above threshold for 12 nuclei from Cl^{37} to Nb^{93}. For each nucleus the excitation function of the average cross section is a monotonically increasing function of proton energy. At 500 kev above threshold the cross sections vary from 40 mb for Cl^{37} to 5×10^{-4} mb for Nb^{93}. One new threshold, that for $Se^{77}(p,n)Br^{77}$, was found to be 2.175±0.004 Mev. In the course of calibrating the neutron detector with an Sb-Be source, a new determination was made of the Sb^{124} half-life: 59.9±0.5 days.

A black-nucleus square-well model was used to compute the cross sections for formation of the compound system. The Coulomb penetrabilities that appear in this calculation qualitatively account for the very large range of cross sections observed. In a more detailed comparison compound-nucleus formation was assumed, and the Hauser-Feshbach formalism was used to include the effects of proton and, especially, γ-ray emission from the compound nucleus. In general, there is agreement with the shapes of the excitation functions but not always with the magnitudes. The ratio of observed to black-nucleus cross-section peaks up by about a factor of 2 between Cu^{65} and Se^{82}. The maximum in the peak is between masses 70 and 75. This peak may be correlated (by a complex-potential model) with a peak in the strength function for s-wave protons and, to a lesser extent, with a peak in the strength function for d-wave protons. Proton strength functions were calculated for a complex square-well of radius $R=1.45A^{\frac{1}{3}}\times10^{-13}$ cm with the approximation of a Coulomb potential constant inside the well and equal to $(4/3)(Ze^2/R)$. In order to fit the observed position of the peak, $A\sim70$ to 75, the depth of the specifically nuclear part of the well was required to be 46 Mev, 4 Mev deeper than the neutron well of Feshbach, Porter, and Weisskopf.

I. INTRODUCTION

CONSIDERABLE evidence now exists that neutron and proton elastic scattering cross sections averaged over resonances are described by the optical model,[1,2] that is, by an average complex potential. The complex potential also, by virtue of its imaginary part, predicts a cross section for formation of the compound system, σ_c;[3] but, by itself, it does not predict the partial cross section for a particular mode of decay once the compound system is formed. Even when reasonable assumptions, for example, that the compound system is a compound nucleus, are made to predict the partial cross sections for decay, special experimental techniques are usually required to observe them. The most abundant data bearing on σ_c at the present time are measurements of the strength function $\langle\Gamma_n^0\rangle/D$ with neutrons in the ev or kev energy region.[3,4] For neutron energies of the order of 1 Mev the compound system often decays by neutron re-emission so that a part of σ_c is confused with shape elastic scattering. For neutron energies above about 4 Mev, compound elastic scattering becomes negligible, and σ_c reduces to the inelastic collision cross section. Measurements are then difficult but interpretations are simplified. It was found[1,5] that the complex square well gives a poor prediction of σ_c; but recently the diffuse-boundary potential, which has also been used for proton scattering,[2] has given a good account of inelastic collision cross sections[6] and a slightly improved description of the s-wave strength function.[3]

For protons there are very limited measurements of σ_c;[7] however, there are several measurements of partial reaction cross sections. Blosser and Handley,[8] for example, report (p,n) reaction cross sections at 12 Mev for $45\leq A\leq142$. The cross sections fluctuate from one nucleus to the next and in each case give only a lower limit to σ_c. From 3 to 6 Mev Blaser *et al.*[9] surveyed (p,n) cross sections for $60\leq A\leq156$. Between adjacent nuclei these also showed fluctuations which were interpreted as variations in σ_c.

If the proton energy is lowered well below the top of the Coulomb barrier but still a few hundred kev above the (p,n) threshold, neutron emission becomes the major decay mode of the compound system. Then σ_c is observed in a straightforward manner by measuring the (p,n) cross section. The present measurements are of (p,n) cross sections averaged over resonances in intermediate nuclei, in each case for energies well below the top of the Coulomb barrier and extending from threshold to about 500 kev above threshold. Earlier[10] thick-target forward-hemisphere yield curves within 100 kev of threshold were accurate only to a factor of 2 but to this accuracy were described by a totally absorbing square-well potential and by the statistical model of the compound nucleus.[11,12] A significant com-

* This work was reported in part at the Washington meeting of the American Physical Society, Bull. Am. Phys. Soc. Ser. II, 2, 177 (1957).
† Summer participant from the University of Michigan.
[1] Feshbach, Porter, and Weisskopf, Phys. Rev. **96**, 448 (1954).
[2] Glassgold, Cheston, Stein, Schuldt, and Erickson, Phys. Rev. **106**, 1207 (1957); Melkanoff, Nodvik, Saxon, and Woods, Phys. Rev. **106**, 793 (1957). References are given to earlier analyses of proton scattering by the optical model.
[3] V. F. Weisskopf, Revs. Modern Phys. **29**, 174 (1957).
[4] H. Marshak and H. W. Newson, Phys. Rev. **106**, 110 (1957).
[5] M. Walt and J. R. Beyster, Phys. Rev. **98**, 677 (1955).
[6] Beyster, Walt, and Salmi, Phys. Rev. **104**, 1319 (1956).
[7] G. H. McCormick and B. L. Cohen, Phys. Rev. **96**, 722 (1954).
[8] H. G. Blosser and T. H. Handley, Phys. Rev. **100**, 1340 (1955).
[9] Blaser, Boehm, Marmier, and Peaslee, Helv. Phys. Acta **24**, 3 (1951); Blaser, Boehm, Marmier, and Sherrer, Helv. Phys. Acta **24**, 441 (1951).
[10] C. H. Johnson and C. C. Trail, Phys. Rev. **93**, 924 (1954).
[11] W. Hauser and H. Feshbach, Phys. Rev. **87**, 366 (1952).
[12] B. Margolis, Phys. Rev. **88**, 327 (1952).

parison of theory and experiment required more accurate cross sections extended further above threshold. The experimental technique for the present measurements is to bombard targets ~20 kev thick (except for Nb^{93}) with analyzed protons and to observe neutrons with a 4π detector of known efficiency. Twenty kev is thick enough to average over many levels of the compound nucleus and thin enough to enable a detailed study of the average excitation function. The experimental details are described in Secs. II and III, and the cross sections are presented in Figs. 2–13. The average standard error other than counting statistics is ±10%.

A major part of the discussion in Sec. IV is devoted to the relation of the average (p,n) cross section, $\sigma_{p,n}$, to σ_c when the statistical assumption of a compound nucleus is made. Once the relation is established one may, in principle, find the parameters of a complex potential which describe the data. We simply report (Fig. 15) the ratios of the observed $\sigma_{p,n}$ to those predicted by a totally absorbing square well of depth 40 Mev and radius $1.45\,A^{\frac{1}{3}}\times10^{-13}$ cm. These ratios are essentially what the complex potential must describe. Following Schiffer and Lee[13] and Margolis and Weisskopf,[14] whose results are in qualitative agreement with ours, we then discuss Fig. 15 in terms of an approximate square-well calculation of proton strength functions.

II. EXPERIMENTAL PROCEDURE

Protons from an electrostatic accelerator were analyzed to ±0.1% by a 60° bending magnet which was calibrated by proton magnetic resonance against the $V^{51}(p,n)Cr^{51}$ threshold.[15] The beam was collimated on the target by two 0.5-in. diameter Ta apertures and four larger antiscattering apertures. The target formed the end of a Faraday cup 1 in. in diameter and 12 in. long. Proton charge was measured by a current integrator to an accuracy better than ±1%.

A 4π detector for neutrons consisted of $B^{10}F_3$ counters imbedded in paraffin surrounding the target. The paraffin moderator was a cadmium-covered cube 17 in. on a side with an additional 2-in. layer of paraffin on the outside. The Faraday cup, which was made of Al to minimize neutron capture, projected into a hole 14 in. deep and 2 in. in diameter centered in one face so that the target was at the cube's center. Seven 1-in. by 6-in. 1-atmos $B^{10}F_3$ counters were imbedded in the paraffin symmetrically situated on a 4.4-in. diameter circle around the beam axis and were operated in parallel with a conventional stabilized power supply and linear amplifier. A comparison of counting rates produced by an intense (10-mC) Co^{60} gamma-ray source and a weak (10^3/sec) Po-Be neutron source dictated a low counter voltage and a high pulse-height bias for maximum gamma-ray discrimination. At frequent intervals the counting rate of a Po-Be source placed at the normal target position was measured in order to check the stability of the entire counting system. When the counting rate differed by as much as 1% from that of the preceding check (after correcting for the decay rate of Po), a slight adjustment was made in the pulse-height bias to bring the two counting rates into agreement.

Neutrons produced at the center of this assembly are thermalized and detected with relatively high efficiency, whereas background neutrons from the outside are strongly attenuated. Since thermalized neutrons are often lost by capture in hydrogen, the counting efficiency depends on the energy and direction of the source neutrons. If the source were strongly anisotropic, the counting rate would depend on angular distribution even though the moderator tends to average over angles. It is assumed here, however, that the (p,n) reactions have sufficiently isotropic yields to make the counting rate a direct measure of the total yield. This should be a good assumption since protons of less than 3 Mev on intermediate nuclei produce small center-of-mass motion and the (p,n) reaction proceeds primarily by compound-nucleus formation.

Since the efficiency as a function of neutron energy cannot be accurately calculated, our first task was to determine it experimentally. This was done by measuring the yield of the $V^{51}(p,n)Cr^{51}$ reaction for six neutron energies from 12 to 700 kev both with the BF_3 counters and with a detector whose relative efficiency is calculable and is, to first approximation, independent of energy. This detector, a Mn bath,[16] was an almost-saturated solution of the $MnSO_4$ in a 50-liter spherical flask with a thin-walled re-entrant Al tube that allowed the V^{51} target to be inserted to the center of the flask. Neutrons produced in the target diffused into the bath and were thermalized and captured by the constituents of the bath, the percentage of the neutrons captured by each constituent being determined by its relative concentration and capture cross section. Neutrons captured in the manganese produce a 2.56-hour activity which is directly proportional to the total neutron yield. The important feature of the detector is that for energies where only scattering is important the bath can be made large enough so that all the neutrons are thermalized and then captured. The specific activity is then independent of the initial neutron energy and direction. Because the 2.56-hour half-life limits the number of measurements to one or two per day, it was much more convenient for the remainder of the (p,n) cross-section measurements to use the BF_3 counters calibrated by comparison with the Mn bath rather than the bath itself.

[13] J. P. Schiffer and L. L. Lee, Jr., Phys. Rev. **107**, 640 (1957).
[14] B. Margolis and V. F. Weisskopf, Phys. Rev. **107**, 641 (1957), and B. Margolis (private communication).
[15] Gibbons, Macklin, and Schmitt, Phys. Rev. **100**, 167 (1955).
[16] R. F. Taschek and A. Hemmendinger, Phys. Rev. **74**, 373 (1948).

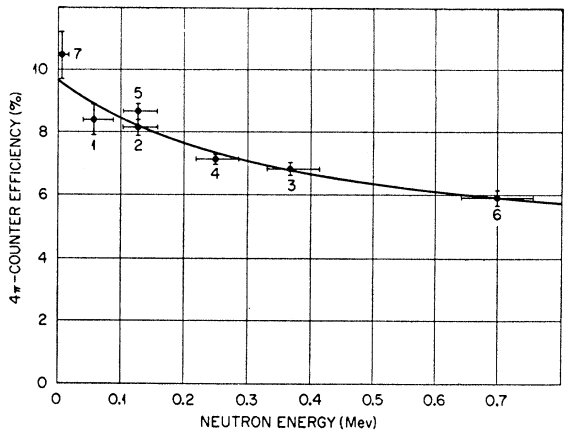

FIG. 1. Efficiency as a function of neutron energy for the 4π-detector consisting of seven BF_3 counters in paraffin. The solid curve has a $\pm 10\%$ uncertainty for energies below 75 kev and $\pm 6\%$ for higher energies.

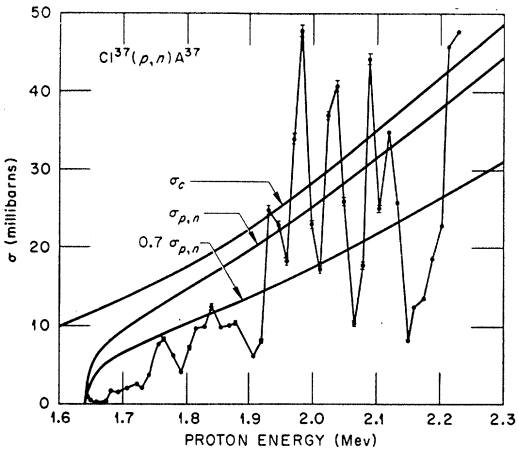

FIG. 2. The cross section for $Cl^{37}(p,n)A^{37}$. The following statements refer to this figure and also to Figs. 3 to 13. The observed cross section is averaged over the target thickness, ~20 kev (excepting Nb^{93}). The flags indicate the standard error resulting from counting statistics if they are larger than the points themselves. The average standard error from all other sources is $\pm 10\%$. The curve labeled σ_c is the cross section for formation of the compound nucleus calculated for a totally absorbing square well of depth 40 Mev and radius $1.45\ A^{\frac{1}{3}} \times 10^{-13}$ cm. The curve labeled $\sigma_{p,n}$ was determined from σ_c with the additional assumption of the statistical model of the compound nucleus. Parameters for the model are given in Table I. The $\sigma_{p,n}$ curve is multiplied by an arbitrary factor (0.7 for Cl^{37}) to force average agreement with the data.

First the yield of the $V^{51}(p,n)Cr^{51}$ reaction at energy intervals of about half the target thickness (22 kev/2) was observed with the BF_3 counters. For the long ($\sim\frac{1}{2}$ hr) Mn bath irradiations proton energies were chosen, indicated by the arrows in Fig. 4, where the yield was insensitive to small fluctuations in proton energy. Then the bath was positioned around the target and activations indicated by the sequence of points 1 to 6 in Fig. 1 were made over a period of several days. After each irradiation the solution was thoroughly stirred and a 7.5-liter sample was transferred to an enclosure shielded by 4 inches of lead where the 845-kev γ-ray of Fe^{56} was counted in a NaI spectrometer and 20-channel pulse-height analyzer. Following these irradiations the yield curve was remeasured with the BF_3 counters. Finally, a thinner target (12 kev) was substituted and the same counter-bath-counter sequence followed to obtain point 7. The absolute efficiency was determined by activating the bath, both preceding and following the above measurements, with a calibrated[17] Sb-Be source, which was placed at the normal target position in the center of the flask.

Figure 1 shows the efficiency of the BF_3 counters *versus* neutron energy. The horizontal bars give the total spread in neutron energy caused by center-of-mass motion and target thickness. Since the yield curve has some structure, several yield curves were obtained to check the reproducibility. The vertical bars on the points in Fig. 1 are primarily a measure of this reproducibility. Counting statistics contribute appreciably only to point 7, near threshold. The efficiencies were obtained with the assumption of negligible neutron leakage from the Mn bath. A calculation based on diffusion theory and Fermi age theory modified for water indicates that the leakage increases by only 2.5% in going from Sb-Be neutrons (27 kev) to 500-kev neutrons.[18] In addition there is a known systematic uncertainty of $\pm 3.2\%$ in absolute calibration arising from $\pm 1.7\%$ in the original NBS Ra-Be standard, $\pm 2.5\%$ in the comparison of our source to that standard and in the decay of the Sb-Be source after its calibration, and $\pm 1\%$ in the activation of the Mn bath. Finally, since the moderator material has no resonances in this energy region, a smooth curve is drawn in Fig. 1 and a combined rms error of $\pm 10\%$ for $E_n < 75$ kev and $\pm 6\%$ for $E_n > 75$ kev is assigned because of the above-mentioned uncertainties.

A by-product of this investigation of errors is a new determination of the Sb^{124} half-life.[19] One Sb-Be source was compared with the National Bureau of Standards Ra-Be standard to $\pm 1.5\%$ in September, 1955, and another Sb-Be source was compared to $\pm 2.0\%$ in June, 1956. These substandards were then intercompared by the Mn bath with good statistics to obtain the half-life, 59.9 ± 0.5 days.

III. EXPERIMENTAL CROSS SECTIONS

A. Results

The object of this experiment is the measurement of average cross sections. The points in Figs. 2–13 give the observed (p,n) cross sections in order of increasing

[17] We are indebted to J. Chin and J. A. De Juren of the National Bureau of Standards for the calibration of two Sb-Be sources.

[18] We are indebted to H. Specter, B. M. Rothleder, and C. R. Kalina of the Massachusetts Institute of Technology Engineering Practice School at Oak Ridge for experimental measurements and theoretical estimates of this leakage.

[19] J. J. Livingood and G. T. Seaborg, Phys. Rev. **52**, 135 (1937).

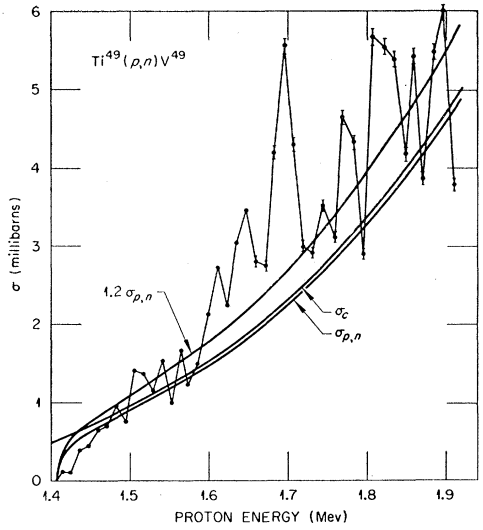

FIG. 3. The $Ti^{49}(p,n)V^{49}$ cross section. See caption for Fig. 2.

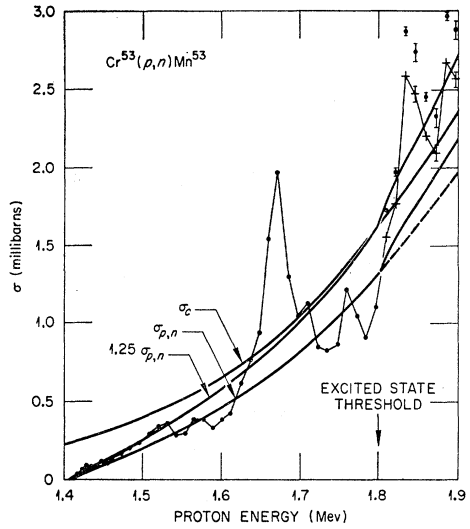

FIG. 5. The $Cr^{53}(p,n)Mn^{53}$ cross section. See caption for Fig. 2. The threshold for the first excited state in the residual nucleus is indicated. The dashed curve was calculated by ignoring the neutrons to the excited state and the solid curve by including them. The data given by crosses have been corrected by 10% to account for the presence of the lower-energy neutron group.

atomic weight for the twelve nuclei listed in Table I. Although some fine structure is present in these excitation functions, it is clear that the targets have been thick enough to provide considerable averaging over resonances, and, except for Cl^{37}, to indicate the course of the average excitation functions—in each case a smooth, monotonic rise. The flags indicate the standard statistical errors if they are larger than the points themselves. Background corrections made from observations with a clean Pt blank were generally negligible except near threshold. For Se^{82} the corrections were 50, 8, and 3% at 1.0, 1.25, and 1.5 Mev, respectively. For both Se^{82} and Nb^{93} the room background was so large that only upper energy limits are assigned to the thresholds. These limits are 930 kev for Se^{82} and 1300 kev for Nb^{93}. One new threshold, that for $Se^{77}(p,n)Br^{77}$, was found to be 2175±4 kev.

B. Target Errors

Column 2 of Table I gives the isotopic abundance of each target. Only the Se isotopes are enriched.[20] Target

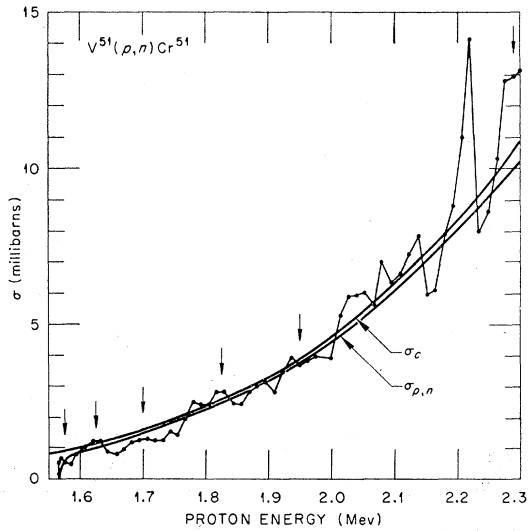

FIG. 4. The $V^{51}(p,n)Cr^{51}$ cross section. See caption for Fig. 2. Here the factor is unity to fit $\sigma_{p,n}$ to the average cross section. Arrows indicate calibration points used for the efficiency curve, Fig. 1.

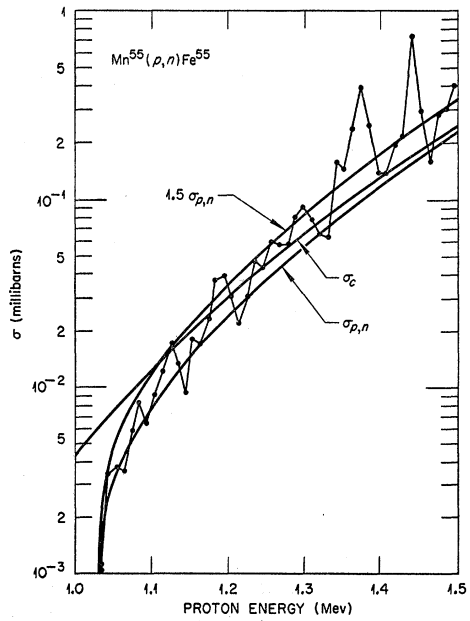

FIG. 6. The $Mn^{55}(p,n)Fe^{55}$ cross section. See caption for Fig. 2.

[20] The selenium isotopes were obtained from the Stable Isotopes Division, Oak Ridge National Laboratory, Oak Ridge, Tennessee.

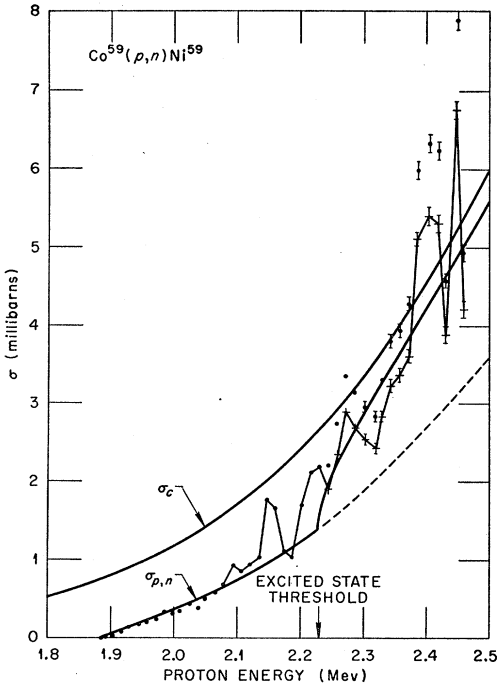

FIG. 7. The $Co^{59}(p,n)Ni^{59}$ cross section. See captions for Figs. 2 and 5. The factor is unity to fit $\sigma_{p,n}$ to the average cross section. The data given by crosses have been corrected by 15% to account for the presence of the lower-energy neutron group.

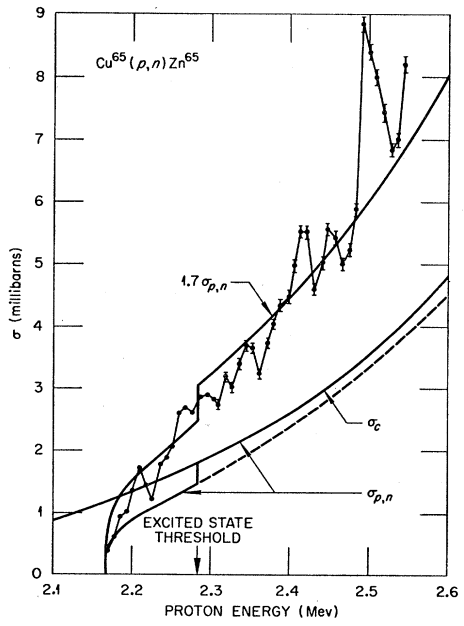

FIG. 8. The $Cu^{65}(p,n)Zn^{65}$ cross section. See caption for Fig. 2. In this figure and also Figs. 9, 10, and 11, the threshold for the first excited state in the residual nucleus is indicated. The dashed curve was calculated by ignoring neutrons to the excited state, and the solid curve by including them. The data are obtained by assuming that all neutrons go to the ground state; it is estimated that the points at the upper energy limit should be lowered by 5±3% because of lower-energy neutron groups.

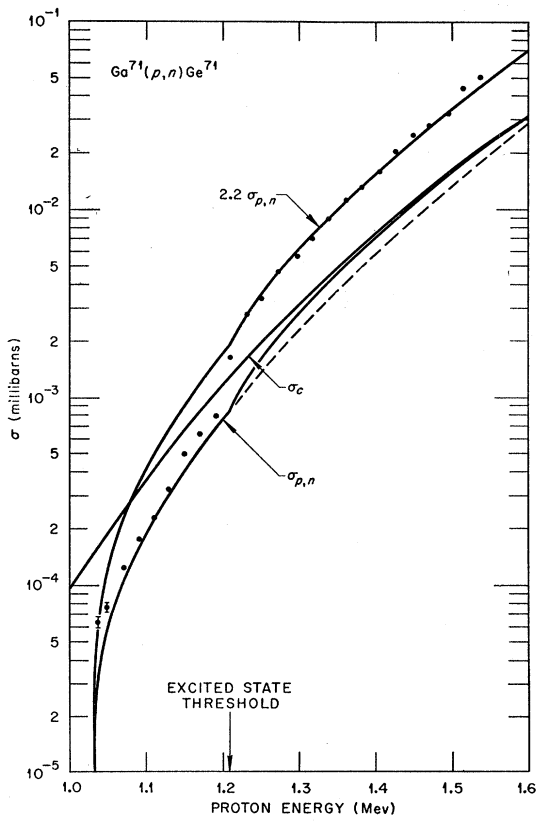

FIG. 9. The $Ga^{71}(p,n)Ge^{71}$ cross section. See captions for Figs. 2 and 8.

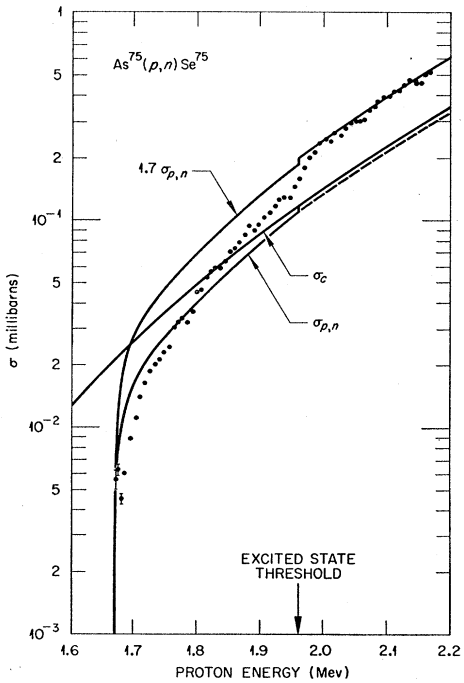

FIG. 10. The $As^{75}(p,n)Se^{75}$ cross section. See captions for Figs. 2 and 8.

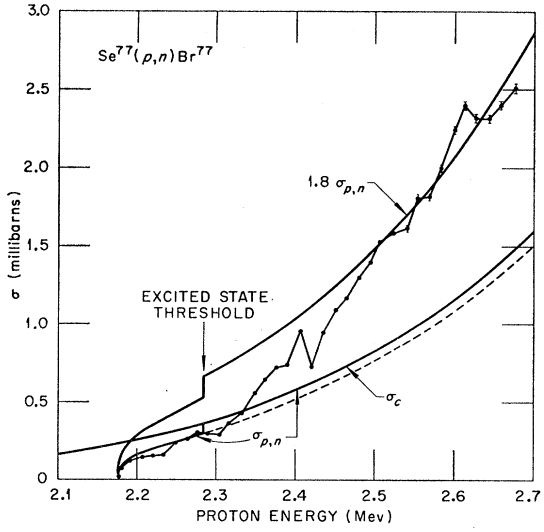

FIG. 11. The $Se^{77}(p,n)Br^{77}$ cross sections. See captions for Figs. 2 and 8.

materials are in elemental form except Cl which is NaCl. All targets except the thick Nb target were evaporated in vacuum from Ta or W filaments onto 0.01-in. thick Pt disks which were cleaned by rubbing with a Ruby eraser, cleaning with solvents, and flaming. Column 3 of Table I lists target thicknesses in mg/cm². Weighing uncertainties are ±2%. Evaporations for the first nine targets were made with a filament-to-target spacing such that ambiguities resulting from nonuniformities are less than ±1%. Because of a limited supply of the separated isotopes of Se^{77} and Se^{82}, the spacing was reduced to the extent that this error is ±3%.

For the selenium targets further nonuniformity developed during the experiments because selenium was readily evaporated by the proton beam. Two targets of each Se isotope were used with currents generally less than 1 μa, and frequent checks were made on reproducibility. For Se^{77} no evaporation was observed for points above 2450 kev; however, points below 2450 kev have an "evaporation" uncertainty of ±5%. More serious evaporation was observed for Se^{82} because larger currents were required near threshold. Since this was anticipated, the yield curve was run with decreasing energy starting with a very weak current near the highest energy of the curve and returning regularly to this point to monitor the target evaporation. This procedure provided a 20±5% evaporation correction below 1100 kev.

The Se^{77} target contained 3% Se^{82}, which has the lower threshold. A correction averaging 7% for the Se^{82} was obtained by extrapolation of its observed yield to higher energies. Another isotope, Se^{80}, having a 19.6% abundance in the Se^{77} target, has a threshold predicted to be 2.7 Mev;[21] therefore, the yield curve was terminated at this energy. A ±7% average uncertainty in the target thicknesses for the selenium targets is obtained for a root-mean-square combination of these errors.

The data for $Nb^{93}(p,n)Mo^{93}$ were obtained by differentiating a thick-target excitation function. Each point results from four thick-target yields. In this case the target error is the uncertainty in the atomic stopping power, ±5%.[22]

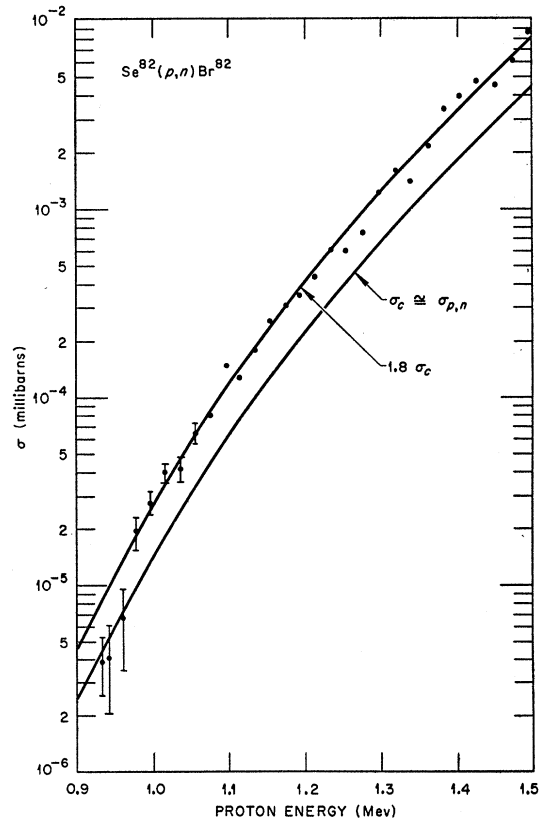

FIG. 12. The $Se^{82}(p,n)Br^{82}$ cross section. See caption for Fig. 2. It is assumed that there are low-lying, low-spin states in Br^{82} so that $\sigma_{p,n} \cong \sigma_c$.

C. Detector Errors

For a given neutron energy the uncertainty in detector efficiency is that of the curve in Fig. 1: ±10% for $E_n < 75$ kev and ±6% for $E_n > 75$ kev. E_n was computed on the assumption that all neutrons went to the residual ground state. This is certainly a correct assumption for proton energies below the neutron threshold for the first-excited state (see Column 7, Table I). Above this threshold some neutrons will go to the excited state and they will be detected with

[21] Way, King, McGinnis, and van Lieshout, *Nuclear Level Schemes, A=40—A=92*, U. S. Atomic Energy Commission Report TID-5300 (U. S. Government Printing Office, Washington, D. C., 1955).

[22] Ward Whaling (private communication to P. H. Stelson). Stopping powers for Nb were found by interpolation between Cu and Ag.

higher efficiency (see Fig. 1) than those which go to the ground state. As discussed in Sec. IV. C, the error in the cross sections introduced by neglecting excited state neutrons was less than 10%, except for $Cr^{53}(p,n)Mn^{53}$ and $Co^{59}(p,n)Ni^{59}$ where it reached 10% and 15%, respectively. In these two cases the existence of excited-state neutrons was included in the calculations. The corrected data are the crosses in Figs. 5 and 7.

IV. COMPARISON WITH BLACK-NUCLEUS MODEL

A. Cross Section for Formation of the Compound System

For cross sections averaged over resonances the interaction between proton and target nucleus may be described by a potential with cross section for formation of the compound system[1,3]

$$\sigma_c=\sum_l \sigma_c{}^l=(\pi/k^2)\sum_l(2l+1)T_l, \qquad (1)$$

where $l\hbar$ is the relative orbital angular momentum of the proton and target, k is the proton wave number, and T_l is a transmission coefficient which is found by matching the wave function inside the nucleus with the Coulomb wave function outside.[23] The nuclear potential has a diffuse boundary and must be complex to allow for proton absorption. The calculation of T_l is difficult; however, one expects with even a crude approximation to the potential that the Coulomb and centrifugal barrier will account for the observed gross variations in cross section (a factor of 5×10^7 from Nb^{93} to Cl^{37}).

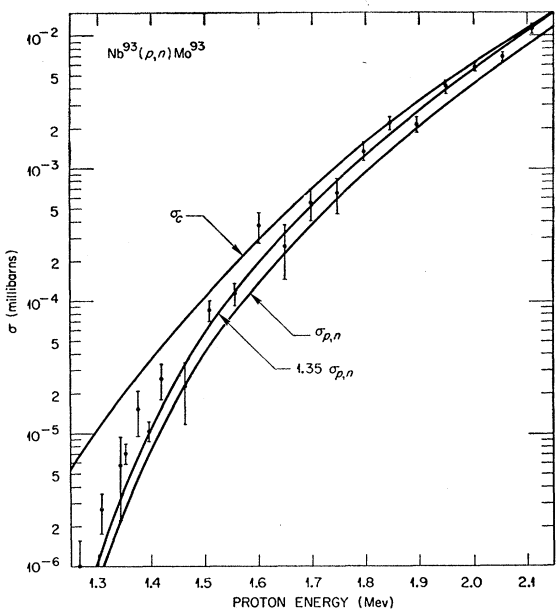

FIG. 13. The $Nb^{93}(p,n)Mo^{93}$ cross section obtained by differentiating a thick-target yield curve. See caption for Fig. 2.

As an approximation which allows easy computation of T_l we assume a totally absorbing square well. Then we have[23]

$$T_l=\frac{4s_lKR}{\Delta_l{}^2+(s_l+KR)^2}, \quad s_l=\frac{kR}{A_l{}^2}, \quad \Delta_l=\frac{kR}{A_l}\frac{dA_l}{d(kr)}\bigg|_{r=R}, \qquad (2)$$

TABLE I. The first three columns list target nuclei with their isotopic abundances and areal densities. The last seven columns list parameters required in Sec. IV B for the statistical theory of the compound nucleus.

1	2	3	4	5	6	7	8	9	10
Target isotope	Percent abundance	Target thickness (mg/cm²)	Initial J^π	Final nucleus	Final J^π	First excited state of final nucleus energy (Mev) J^π	$2\pi\Gamma_r/D$ Dresner[k]	$2\pi\Gamma_r/D$ Cameron[l] Newton[m]	D^{J-I} Newton[m]
Cl^{37}	24.6	0.193	$3/2^+$[a]	A^{37}	$(3/2^+)$[a]	1.41[e]	0.3	0.19	40
Ti^{49}	5.51	0.159	$7/2^-$[b]	V^{49}	$(7/2^-)$[b]	0.089 $(5/2^-)$[b]	0.7	9.5	0.3
V^{51}	99.76	0.230	$7/2^-$[b]	Cr^{51}	$(7/2^-)$[b]	0.74[b]	0.8	6.4	0.5
Cr^{53}	9.55	0.147	$3/2^-$[b]	Mn^{53}	$7/2^-$[c]	0.38[b] $(5/2^-)$[f]	0.9	3.4	1
Mn^{55}	100	0.114	$5/2^-$[b]	Fe^{55}	$(3/2^-)$[b]	0.42[b]	1.1	0.84	4
Co^{59}	100	0.261	$7/2^-$[b]	Ni^{59}	$(3/2^-)$[b]	0.34[e,g] $(7/2^-)$[b]	1.5	1.76	2
Cu^{65}	30.9	0.243	$3/2^-$[b]	Zn^{65}	$(5/2^-)$[b]	(0.052) 0.119[h]	2.0	0.55	8
Ga^{71}	39.8	0.204	$3/2^-$[b]	Ge^{71}	$(1/2^-)$[b]	0.175[b]	3.0	0.57	9
As^{75}	100	0.202	$3/2^-$[b]	Se^{75}	$5/2^+$[d]	0.286[i]	4.5	10.7	0.2
Se^{77}	49.4	0.240	$1/2^-$[b]	Br^{77}	$(3/2^-)$[b]	0.107[b]	5.0	5.3	0.4
Se^{82}	75.74	0.218 0.175 0.185	0^+[b]	Br^{82}	(6^-)[b]	low[b]	7.0	2.9	0.6
Nb^{93}	100	thick	$9/2^+$[a]	Mo^{93}	$(5/2^+)$[a]	1.46[j]	10.0	16.5	0.07

[a] P. F. A. Klinkenberg, Revs. Modern Phys. **24**, 63 (1952).
[b] See reference 21.
[c] Dobrowski, Jones, and Jeffries, Phys. Rev. **104**, 1378 (1956).
[d] L. C. Aamodt and P. C. Fletcher, Phys. Rev. **98**, 1224 (1955).
[e] See reference 32.
[f] See reference 33.
[g] Butler, Dunning, and Bondelid, Phys. Rev. **106**, 1224 (1957). The weak neutron group reported for $Co^{59}(p,n)Ni^{59}$ and leaving Ni^{59} in a 439-kev state is neglected in our calculations.
[h] See reference 30.
[i] J. W. Butler and C. R. Gossett, Bull. Am. Phys. Soc. Ser. II, **2**, 230 (1957).
[j] See reference 31.
[k] See reference 26.
[l] See reference 28.
[m] See reference 27.

[23] J. M. Blatt and V. F. Weisskopf, *Theoretical Nuclear Physics* (John Wiley and Sons, Inc., New York, 1952), p. 360.

where K is the proton wave number within the well, R is the radius of the well, and A_l^{-2} is the Coulomb penetrability. Since the proton energy for these (p,n) reactions is always well below the Coulomb barrier, the Coulomb penetrability, which is the controlling factor in the numerator of the expression for T_l, is much less than unity and depends critically on proton energy and nuclear radius. In the denominator s_l is completely negligible compared to KR, and Δ_l^2 is about 8, 10, and 15% of $(KR)^2$ for s-, p-, and d-wave protons, respectively. A_l^{-2} and Δ_l^2 for $l=0$ to 4 were obtained to an accuracy of 1 to 2% from graphs constructed from published tables of Coulomb wave functions.[24] When values of T_l are calculated in this manner and inserted into the cross-section formula, Eq. (1), the partial cross sections for $l=0$, 1, 2, and 3 are approximately 44, 44, 11, and 1%, respectively, for the lightest nucleus studied and 31, 48, 18, and 3% for the heaviest.

In the 12 cross-section curves, Figs. 2 to 13, the black-nucleus cross section, σ_c, for formation of the compound system is presented for a 40-Mev square well with $R=1.45\,A^{\frac{1}{3}}\times10^{-13}$ cm. These curves give a good account of the gross variations in cross section but fail to reproduce the detailed average cross sections in two respects. First, the average experimental cross section generally falls more rapidly with decreasing energy than does σ_c. This deviation in shape is clearly the result of competing reactions which are particularly effective near threshold. Second, for several of the figures, notably for $65\leq A\leq82$, the average experimental cross section rises above σ_c. Since a (p,n) cross section cannot exceed that for formation of the compound system, the crude approximation of a totally absorbing square well is inadequate. To seek better agreement between theory and experiment we proceed first to the relation of $\sigma_{p,n}$ to σ_c, that is to a closer study of the shapes of the curves. Then, in Sec. IV it is shown that the necessary increase in magnitude for $65\leq A\leq82$ is provided by a complex potential.

B. Decay of the Compound System: Competing Reactions

The relation of $\sigma_{p,n}$ to σ_c is an additional problem since the complex potential predicts only the formation of the compound system without reference to the subsequent decay. The extra assumption introduced here is that the compound system is a compound nucleus whose decay is described by the statistical nuclear model.[11] Then

$$\sigma_{p,n}=\sum_l \sigma_{p,n}{}^l=\sum_l \sigma_c{}^l \sum_J g_J{}^l\left(\frac{\Gamma_n{}^J}{\Gamma_n{}^J+\Gamma_p{}^J+\Gamma_r{}^J}\right), \quad (3)$$

where the ratio of the Γ's is the ratio of the decay rate for neutron emission to that for all processes—neutron, proton, and γ-ray emission. The sum is over all states in the compound nucleus of total angular momentum, J, formed by each l, and $g_J{}^l$ is a statistical weight factor:

$$g_J{}^l=\frac{2J+1}{2(2I+1)(2l+1)}\epsilon_{jl}{}^J, \quad (4)$$

where I is the spin of the target nucleus, j is the channel spin $I\pm\frac{1}{2}$, and $\epsilon_{jl}{}^J$ is 2, 1, or 0 depending on whether both, one, or neither of the channel spins can combine with l to form J. Since $\sum_J g_J{}^l=1$, $\sigma_{p,n}$ approaches σ_c whenever $\Gamma_n{}^J\gg(\Gamma_p{}^J+\Gamma_r{}^J)$. Column 4 of Table I lists the measured spins and assumed parities of the initial ground states.

1. Proton Re-Emission

In general, but not always, neutron emission predominates. Hauser and Feshbach[11] show by reciprocity (assuming no excited states available for neutrons or protons) that

$$\frac{\Gamma_p{}^J}{\Gamma_n{}^J}\cong\frac{\epsilon_{j'l'}{}^J T_{l'}(E_p)}{\epsilon_{j''l''}{}^J T_{l''}(E_n)}, \quad (5)$$

where E_p and E_n are proton and neutron energies in the center-of-mass system, the primes indicating outgoing channels. The final nuclei are listed in Table I, Column 5, and their spins and parities, from which the l'' and j'' are determined, in Column 6. Only Mn^{53} and Se^{75} have measured spins. The approximation sign is ours, and refers to the fact that only the terms for lowest l' and l'' are included. This approximation is good, because parity conservation requires that higher l values increase in steps of 2, and for the energies encountered here the T_l are rapidly decreasing functions of l. When excited states become available in the target and residual nucleus, additional terms appear in the numerator and denominator. Excited states in the target nucleus are not important because the Coulomb barrier strongly favors the ground state; however, in some cases to be noted excited states in the residual nucleus are important. Column 7 lists the lowest known excited states in the final nucleus; Br^{82} is assumed to have low-lying, low-spin states.[21] Since proton re-emission is small, $\Gamma_p{}^J/\Gamma_n{}^J$ was calculated from Eqs. (2) and (5) with the approximation that Δ_l and s_l in the denominator of Eq. (5) were zero.

2. Gamma-Ray Emission

The γ-ray competition factor, $\Gamma_r{}^J/\Gamma_n{}^J$, which is usually larger than the proton factor, was evaluated semiempirically from rather limited data on neutron capture. Following Margolis,[12] we write

$$\frac{\Gamma_r{}^J}{\Gamma_n{}^J}\cong\frac{2\pi\Gamma_r{}^J/D^J}{\epsilon_{j''l''}{}^J T_{l''}(E_n)}, \quad (6)$$

[24] Bloch, Hull, Broyles, Bouricius, Freeman, and Breit, Revs. Modern Phys. 23, 147 (1951) and *Tables of Coulomb Wave Functions*, National Bureau of Standards Applied Mathematics Series 17 (U. S. Government Printing Office, Washington, D. C., 1952).

where D^J is the average spacing of levels of given J and parity at the appropriate excitation energy of the compound nucleus. Here again we have included only the lowest l'' value for the neutron and have assumed neutron emission only to the ground state.

Margolis[12] presents arguments that $2\pi\Gamma_r{}^J/D^J$ is independent of J. The most extensive data on neutron capture cross sections for medium-weight nuclei are those of Hughes *et al.*[25] for an effective neutron energy of 1 Mev. Dresner[26] extracted $2\pi\Gamma_r/D$ from Hughes' data, using an approximation which gives agreement with the Margolis analysis to about a factor of 2. These values of $2\pi\Gamma_r/D$ do not, however, belong to the compound nuclei formed in our (p,n) reactions. Many of the same target nuclei were used in both Hughes' work and ours, but in his case a neutron was added, and in ours a proton. For the two sets of compound nuclei the effective excitation energies[27] were computed. With four of our targets, $A=37$ to 53, the difference in the effective excitation energy upon adding either a neutron at 1 Mev or a proton at the (p,n) threshold is only ~ 1 Mev, and with the other eight targets it is much less. The sensitivity of $2\pi\Gamma_r/D$ to energy is, perhaps, a factor-of-two per Mev.[12,26] As a knowledge of $2\pi\Gamma_r/D$ to an accuracy of a factor of 5 is adequate in the present work, our assumed values (Column 8, Table I) were taken from a smooth curve through Dresner's points.

In order to check these values against gross errors, we have also computed $2\pi\Gamma_r{}^J/D^J$ from the semi-empirical formulas of Newton[27] and Cameron[28] and from the binding energies of Wapstra.[29] The compound nuclei and excitation energies were those formed in the (p,n) reactions at threshold. Although we have assumed no J-dependence, we note that J does enter into these semiempirical values through Newton's level spacing, $D^J=(2J+1)^{-1}D_0$. Since $l_p \leq I$ (hence $J_{\text{average}}=I$) in most of our work, we have obtained a suitable average by setting $J=I$. The results, Column 9 of Table I, show an average agreement with the values obtained from Dresner's work, but also show marked differences for some of the nuclei. These differences arise chiefly from a dependence of D on shell effects which are not well established in this mass region.[27] To illustrate, we tabulate separately the average level spacing, $D^{J=I}$, in Column 10 of the table and make a qualitative comparison with the spacing of peaks in our yield curves. These peaks do not, of course, result from individual resonances; nevertheless, they reflect the actual level-spacing and its change from one nucleus to the other. A comparison shows that the predicted shell dependence for D is not entirely correct. For example, it is predicted that the spacing for $Ti^{49}(p,n)V^{49}$ is 27 times smaller than that for $Cu^{65}(p,n)Zn^{65}$; whereas the Ti^{49} yield actually shows stronger fluctuations than does that for Cu^{65}. It is predicted that the level spacing for $Ga^{71}(p,n)Ge^{71}$ is slightly greater than for $Cu^{65}(p,n)Zn^{65}$, whereas the Ga^{71} curve is much smoother than that for Cu^{65}. Thus the local fluctuations of the predicted $2\pi\Gamma_r{}^J/D^J$ are not really significant.

[25] Hughes, Spatz, and Goldstein, Phys. Rev. **75**, 1781 (1949).
[26] L. Dresner, J. Nuclear Energy **2**, 118 (1955).
[27] T. D. Newton, Can. J. Phys. **34**, 804 (1956).
[28] A. G. W. Cameron, Can. J. Phys. **35**, 666 (1957).
[29] A. H. Wapstra, Physica **21**, 385 (1955).

C. (p,n) Cross Sections

We have used values of $g_J{}^l$, $\Gamma_p{}^J/\Gamma_n{}^J$, and $\Gamma_r{}^J/\Gamma_n{}^J$ as discussed above to obtain $\sigma_{p,n}$ from Eq. (3). The results are the curves labeled $\sigma_{p,n}$ in Figs. 2 to 13. The dashed curves shown in some of the figures for energies above excited-state thresholds were calculated by neglecting the excited states, and the solid curves by including them. It is seen that the $\sigma_{p,n}$ curves usually agree with the average excitation functions in shape, but not often in magnitude. The relation of $\sigma_{p,n}$ to σ_c and the importance of excited states show a strong dependence on the relative spins of initial and final ground states because the larger the spin change the greater the inhibition of neutron emission relative to proton and γ-ray emission. It is convenient, therefore, in the following discussion to group the curves according to the spin change from initial to final nucleus.

1. Initial and Final Nuclei of Same Spin and Parity

This includes Cl^{37}, Ti^{49}, V^{51}, and in a sense Se^{82}. We illustrate with $V^{51}(p,n)Cr^{51}$. States formed by s-wave protons can decay by emission of s-wave neutrons. For these the penetrability rises so quickly that $\sigma_{p,n}{}^0$ is nearly $\sigma_c{}^0$ at 2 kev above threshold. States formed by p-wave protons can decay by emission of p-wave neutrons which experience competition with protons and γ rays for a greater energy above threshold; however, at 50 kev above threshold $\sigma_{p,n}{}^1$ has risen to $0.9\sigma_c{}^1$. States formed by d-wave protons can decay 40% by emission of s-wave neutrons and 60% by emission of d-wave neutrons; thus, $\sigma_{p,n}{}^2$ rises within a few kev to $0.4\sigma_c{}^2$ and then more slowly for about 500 kev to its full value, $\sigma_c{}^2$. Terms with f-wave protons are quite small. In summary, Fig. 4 shows that $\sigma_{p,n}$ rises within 50 kev nearly to σ_c, in good agreement with experiment.

Theoretical curves in Fig. 3 for Ti^{49} are similar to those for V^{51}. Low-lying excited states will have negligible effect since their presence only decreases the gap, which is already negligible, between $\sigma_{p,n}$ and σ_c. When the curve for $\sigma_{p,n}$ is multiplied by a suitable factor (1.25), it shows agreement in both shape and magnitude with the average excitation function.

For $Cl^{37}(p,n)A^{37}$, the reaction with the lightest nucleus of the group, proton re-emission from the compound nucleus becomes appreciable and causes $\sigma_{p,n}$ to fall well below σ_c. In Fig. 2 the curve for $\sigma_{p,n}$ is multiplied by 0.7 to force average agreement in magnitude with the observed excitation function; however, the multiplier is subject to large uncertainty because

the experiment clearly has not averaged over enough resonances.

For Se^{82} the ground state transition, which involves a large spin change (0^+ to 6^-), can contribute very little to the cross section. Since the experimental curve and σ_c have the same shape, it is assumed that there is a low-lying state, probably 0^+, in Br^{82}. In this case $\sigma_{p,n} \cong \sigma_c$, except very near the threshold, whose energy was too low for us to measure.

2. Spins of Initial and Final Nuclei Differ by One Unit

This includes Mn^{55}, Cu^{65}, Ga^{71}, As^{75}, and Se^{77}. The essential difference from no spin change is that only part of the states formed by s- and p-wave protons decay by emission of s- and p-wave neutrons; the rest can emit neutrons only if they are at least d and f waves. Thus, $\sigma_{p,n}$ rises less rapidly toward σ_c. Excited states cannot be ignored because they usually open channels for s- and p-wave neutrons. The cross sections including excited states can be calculated if the spins and parities of the states are known. As an example, $\sigma_{p,n}$ for $Ga^{71}(p,n)Ge^{71}$ is shown in Fig. 9 with the assumption of a single, 175-kev, $5/2^-$ excited state in Ge^{71}.[21] The essential feature of the curve is that the presence of the excited state allows $\sigma_{p,n}$ to rise very nearly to σ_c. It is assumed for Cu^{65}, As^{75}, and Se^{77} that the excited states open channels so that $\sigma_{p,n}$ rises to σ_c; this is indicated in Figs. 8, 10, and 11 by a discontinuity at the excited-state threshold. For Mn^{55} the excited-state threshold (1460 kev) is so near the end of our yield curve that its effect is negligible.

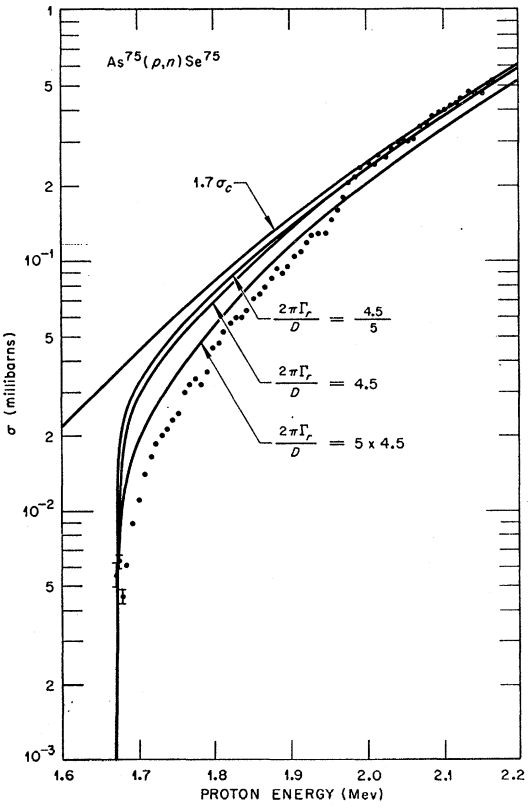

FIG. 14. Curves are shown which indicate the effect of varying $2\pi\Gamma_r/D$ by a factor of 5 each way from "normal" for $As^{75}(p,n)Se^{75}$. All curves are calculated for a black nucleus and multiplied by an arbitrary factor of 1.7.

The presence of lower energy neutron groups makes an error in our experimental cross sections because the detector is energy sensitive. For the above example, $Ga^{71}(p,n)Ge^{71}$, it is predicted that at the upper energy limit of the curve 60% of the neutrons leave Ge^{71} in the excited state. The reported cross sections are then 5% high. The same estimate is made for $As^{75}(p,n)Se^{75}$. For $Cu^{65}(p,n)Zn^{65}$ estimates made from observed neutron groups[30] indicate the cross section is 4% high. It is concluded that our experimental cross sections for Cu^{65}, Ga^{71}, As^{75}, and Se^{77} are $(5\pm3)\%$ high at the upper energy limit because of this effect.

In determining the ratios of observed to calculated cross sections we have weighted the upper energy region more strongly than the lower, because the sensitivity of $\sigma_{p,n}$ to $2\pi\Gamma_r/D$, whose values we do not know very accurately, decreases with energy. The shape of the $\sigma_{p,n}$ curves at the lower energies can usually be brought into perfect agreement with the data by our making a small change in $2\pi\Gamma_r/D$. For Ga^{71}, As^{75}, and Se^{77}, however, the $\sigma_{p,n}$ curves normalized to fit at the upper energies are much too high at the lower energies.

As an example of the effect of increased γ-ray emission on $\sigma_{p,n}$, Fig. 14 shows curves of $1.7\sigma_{p,n}$ for As^{75} calculated with the value of $2\pi\Gamma_r/D$ in Table I, and also with $\frac{1}{5}$ and with 5 times this value. Although the larger value, which is as large as any in Dresner's plot, improves the shape of the curve, it is not enough. One can further increase γ-ray emission, and thus improve the shape, by decreasing the $T_l(E_n)$ in Eq. (6). This approach is reasonable since the $T_l(E_n)$ really are smaller around mass 75 than the black-nucleus values[1] assumed. Another improvement in shape is obtained if the $T_l(E_p)$ are derived from the complex potential discussed in Sec. V. With these additional changes it seems possible that the As^{75} data, and similarly the Ga^{71} and Se^{77} data, could be fitted.

It may be, however, that the compound-nucleus assumption is not quite true and decay through direct interaction plays a significant role. If so, $\sigma_{p,n}$ may not reach σ_c even at 500 kev above threshold, and the factors between observed and black-nucleus cross sections may be larger than those indicated in Figs. 9, 10, 11, and 14. In connection with the possibility of direct interaction, it is interesting to note that the As^{75} data can be fitted if we assume that $\sigma_{p,n}/\sigma_c$ varies as $(E_n)^{\frac{1}{2}}$.

[30] J. B. Marion and R. A. Chapman, Phys. Rev. **101**, 283 (1956); E. M. Bernstein and H. W. Lewis, Phys. Rev. **107**, 737 (1957). These investigators find a low yield of neutrons to the 52-kev state.

The data for $Ga^{71}(p,n)Ge^{71}$ and $Se^{77}(p,n)Br^{77}$ could easily be fitted if we assumed a spin change of two instead of one. The spins of Ge^{71} and Br^{77} have not been measured. This freedom is not allowed for $As^{75}(p,n)Se^{75}$ which is known to have a spin change of one.

3. Spins of Initial and Final Nuclei Differ by Two Units

This includes Cr^{53}, Co^{59}, and Nb^{93}. For each reaction there is no parity change; thus, states formed by *s*-wave protons can emit neutrons only if they are at least *d* waves, and a large fraction of the states formed by *p*-wave protons can emit neutrons only if they are at least *f* waves. Competition of γ rays and protons with neutron emission becomes important for several hundred kev above threshold. The resulting theoretical curves in Figs. 5, 7, and 13 fall well below σ_c.

Excited states will be very important for these cases. For $Nb^{93}(p,n)Mo^{93}$ no excited states are known[31] in our energy region, and the data show no hint of an excited-state threshold. For $Co^{59}(p,n)Ni^{59}$ the solid theoretical curve is found by assuming the 340-kev state[32] in Ni^{59} is $7/2^-$. For energies above the excited-state threshold it is predicted that most of the neutrons leave Ni^{59} in the excited state. From the predicted ratios of the number of excited-state to ground-state neutrons and from our neutron detector's efficiency curve it is found that a 15% correction must be made. For $Cr^{53}(p,n)Mn^{53}$ it is assumed[33] that the 380-kev state is $5/2^-$; the correction above the excited-state threshold is then 10%. These corrections are based on spin and parity assignments which are not well established. For Co^{59}, however, the assignments predict an excited- to ground-state yield ratio of 3.0 for 3.3-Mev protons, in good agreement with the observed ratio of 2.6.[32] In Figs. 5 and 7 the data plotted as crosses have been corrected for the effect of the lower-energy neutron group.

When the $\sigma_{p,n}$ curves for these three reactions are multiplied by suitable numbers (unity for Co^{59}), the agreement with the average excitation functions is good. In fact, the good description obtained for reactions involving a spin change of two units represents one of the more satisfactory results of this investigation.

V. COMPARISON WITH THE COMPLEX-POTENTIAL MODEL

In the last section it was seen that the black-nucleus model did not always predict the correct magnitude for the average (p,n) cross sections. The ratio of observed to predicted cross section is plotted in Fig. 15 as a function of the target mass number. The indicated uncertainties are only rough estimates which attempt to take account of such effects as fluctuating resonance structure, uncertainties in γ-ray emission, and errors in observed cross sections. These estimates do not include the possibility that points for $A=71$, 75, and 77 are too low because of possible failure of the compound-nucleus assumption.

Although the black-nucleus cross section is not sensitive to the depth of the well (varying approximately as its inverse square root), it is very sensitive to the radius. The highest point in Fig. 15, that for $A=71$, would be given the value 1.0 if we chose $R=1.62\,A^{\frac{1}{3}}$. A radius between $1.45\,A^{\frac{1}{3}}$ and $1.62\,A^{\frac{1}{3}}$ would then make the black-nucleus cross sections a fair average of the experimental points. Unlike the (p,n) cross sections at 6 Mev[9] and 12 Mev,[8] which were, in fact, consistent with radii larger than $1.45\,A^{\frac{1}{3}}$, the deviations from the black-nucleus model observed here are not randomly up and down, but are a systematic function of A with a clear-cut maximum for $A\sim65$ to 85. (The maximum at $A=55$ may be spurious, since it is based primarily on one point, that for Co^{59}.)

In going from a black-nucleus to a complex-potential model the only changes in the calculated cross sections occur through modifications in the values of T_l or, since $T\cong 2\pi\langle\Gamma\rangle/D$,[34] in the values of the strength functions. These changes are quite important for the formation of the compound system [Eq. (1)] but, except near threshold, not very important for its decay because neutron emission is so strongly favored. Just as for neutrons, the proton strength functions will have peaks as a function of mass number and these will show up through Eq. (1) in the (p,n) cross sections. We can, therefore, expect that for a properly chosen complex

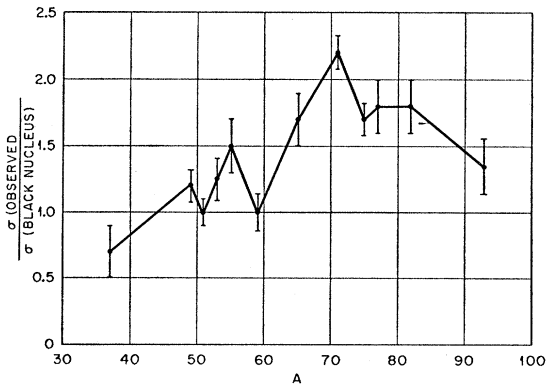

FIG. 15. The ratio of the observed average cross section to the black-nucleus cross section for a 40-Mev square well and a radius $1.45\,A^{\frac{1}{3}}\times10^{-13}$ cm. The ratios are the factors indicated in Figs. 2–13 and are plotted here as a function of A for the target nucleus. Vertical heights of the points are uncertainties estimated very roughly within the framework of the statistical theory of the compound nucleus.

[31] R. Patterson, Phys. Rev. **95**, 303 (1954). The observed Q for the $Nb^{93}(p,n)Mo^{93}$ ground-state transition was used to predict a (p,n) threshold of 1270 kev for use in the theoretical (p,n) cross section of the present paper.

[32] P. H. Stelson and W. M. Preston, Phys. Rev. **86**, 807 (1952).

[33] Way *et al.*[21] assign $5/2^-$ to the Mn^{53} ground state and $7/2^-$ to the first excited state. We invert the order to agree with the measured ground state spin (see Table I).

[34] J. M. Blatt and V. F. Weisskopf, *Theoretical Nuclear Physics* (John Wiley and Sons, Inc., New York, 1952), p. 389.

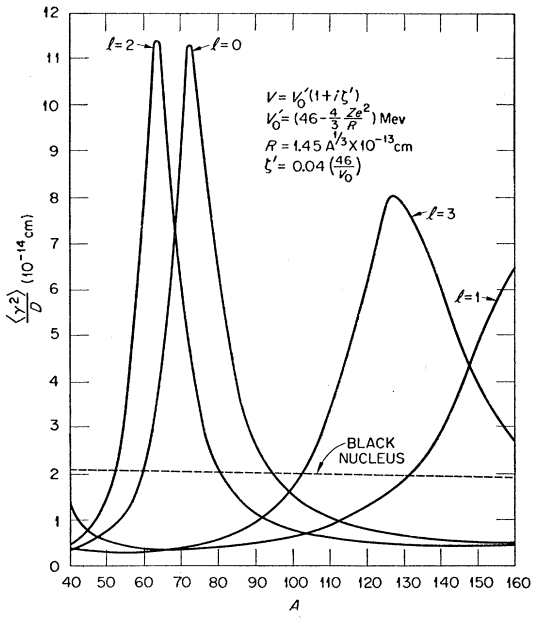

FIG. 16. Strength functions for 2-Mev s-, p-, d-, and f-wave protons *versus* mass number. The calculations are for a complex square well of depth $[46(1+0.04i)-V_c]$ Mev and radius $R=1.45\,A^{\frac{1}{3}}\times10^{-13}$ cm. V_c, the Coulomb potential inside the well, is approximated by a constant for each nucleus: $\frac{4}{5}Ze^2/R$.

potential the broad peak from $A\sim65$ to 85 in Fig. 15 may be fitted.

Indeed, Margolis, and Weisskopf[14] have shown from a Fermi-gas model that the Coulomb potential shifts the shell-model $3s$ peak from $A=55$ for zero-energy neutrons to $A\approx68$ for protons.

We have made a very approximate square-well calculation of the strength functions for s-, p-, d-, and f-wave protons, using a proton energy in the middle of our experimental range, namely 2 Mev. The complex well depth is $V_0(1+i\zeta)-V_c$, where V_0 and ζ are independent of A and $V_c=\frac{6}{5}Z/A^{\frac{1}{3}}$ Mev is the radial average of the Coulomb energy for a uniform charge distribution inside the well whose radius is taken as $R=1.45\,A^{\frac{1}{3}}\times10^{-13}$ cm. Making the Coulomb potential constant inside the nucleus is a big approximation, but it does lead to a simple calculation. The choice of the radial rather than the volume average comes from consideration of the WKB solution.[14]

The well depth may now be rewritten as $V_0'(1+i\zeta')$, where $V_0'=V_0-V_c$ and $\zeta'=\zeta V_0/(V_0-V_c)$. Since this is exactly the form of the well depth for neutrons, the neutron formulas[1] may be, and were, used in calculating[35] the internal logarithmic derivatives, f_l. It is to be noted, however, that because of the dependence on V_c the well depth is changing throughout the periodic table. The strength functions computed from

$$\frac{\langle\gamma_l^2\rangle}{D}\cong\left(\frac{R}{\pi}\right)\frac{-\mathrm{Im}f_l}{(\mathrm{Im}f_l-s_l)^2+(\mathrm{Re}f_l-\Delta_l)^2},\qquad(7)$$

with $V_0=46$ Mev and $\zeta=0.04$, are shown in Fig. 16. Although s_l is negligible, Δ_l, the real part of the logarithmic derivative of the external wave function, is very important in locating the peaks. The inclusion of Δ_l always shifts the peaks to higher mass numbers, the shift increasing with l and with A. The s-wave peak in Fig. 16 was shifted up by 12 mass units in contrast with the case of s-wave neutrons for which $\Delta=0$. The dependence on proton energy is such that a choice of 1.5 Mev instead of 2 Mev for the average proton energy would shift the s-wave peak upward by ~3 mass units. This is small compared to the width of the peak.

The values of V_0 and ζ were chosen to fit the peak in Fig. 15. To see that this has been accomplished we note that at $A\sim72$ the values of $\sigma_c{}^l/\sigma_c$ for a black nucleus are $\cong0.35$, 0.47, and 0.16 for s-, p-, and d-wave protons, respectively. Multiplying these by the strength functions (divided by the black-nucleus value) in Fig. 16 at $A\sim72$, we get $\sigma_c/(\text{black-nucleus }\sigma_c)\cong(0.35)(5.5)+(0.47)(0.19)+(0.16)(2.5)=2.4$, in good agreement with the value of the observed peak. As the sensitivity of the position of the calculated peak to the value of V_0 is ~5 mass units per Mev, it appears that the proton well (46 Mev) is significantly deeper than the neutron well (42 Mev in reference 1), and the difference is about the same as that found in studies of the bound states of nuclei in this mass region.[36]

Details of the strength-function curves cannot be taken too literally because of the above-mentioned Coulomb approximations and because of the use of a nuclear well that is square and of depth constant with A. For an equivalent rounded well we could expect the tails of the strength functions to be raised.[1,3] This modification might raise the strength functions around $A=45$, for example, where the square well (Fig. 16) predicts a (p,n) cross section of only $\frac{1}{3}$ the black-nucleus cross section. Also, the relative positions of the peaks would shift,[37] thus altering, for example, the decomposition of the observed peak into s and d waves. Finally, we note that the difference in the well depths for protons and neutrons is a Coulomb or neutron-excess effect—our V_0 should really increase with A.[36,37] If this were done, the $l=3$ and, even more so, the $l=1$ peaks would be readily shifted to lower mass numbers. Indeed, Schiffer, and Lee[13] may already have observed the f-wave peak at $A\sim110$ and the beginnings of the p-wave peak at $A\sim130$.

[35] We thank Lawrence Dresner of this laboratory for calculating the f_l on the Oracle.

[36] A. E. S. Green, Phys. Rev. **102**, 1325 (1956); **104**, 1617 (1956).

[37] A. E. S. Green and K. Lee, Phys. Rev. **99**, 772 (1955); Ross, Lawson, and Mark, Phys. Rev. **104**, 401 (1956); Ross, Mark, and Lawson, Phys. Rev. **102**, 1613 (1956).